Fabric Defect Detection Based on Membership Degree of Regions

LIWEN SONG[1,3], RUIZHI LI[1,3], AND SHIQIANG CHEN [2,3]
[1]School of Mathematics and Statistics, Hubei Minzu University, Enshi 445000, China
[2]School of Advanced Materials and Mechatronic Engineering, Hubei Minzu University, Enshi 445000, China
[3]Institute of University–Industry Cooperation for Advanced Material Forming and Equipment, Hubei Minzu University, Enshi 445000, China

Corresponding author: Shiqiang Chen (1997013@hbmzu.edu.cn)

ABSTRACT The detection of fabric defects is an important part of fabric quality control, and hence is thus a research hotspot in the textile industry. With the aim of effectively detecting fabric defects, this paper describes an improved fabric defect detection method based on the membership degree of each fabric region (TPA). By analyzing the regional features of fabric surface defects, the saliency of defect regions can be determined using the extreme point density map of the image and the features of the membership function region. A threshold iterative method and morphological processing are used to ensure the precise and accurate detection of fabric defects. Experimental results show that compared with two classical fabric defect detection methods, the proposed detection method can detect fabric defects more effectively while also suppressing the interference of noise and background textures. Additionally, numerical results demonstrate the validity and feasibility of the proposed method to satisfy the requirements of online detection.

I. INTRODUCTION

Many fabric defects occur during the production process of fabrics, such as broken weft, double weft, thin and dense paths, broken warps, jumping flowers, pilling and grease spots. These defects have negative effects on the appearance, comfort, and performance of the fabric. Traditional artificial defect detection is affected by psychological and other subjective conditions. As well as being labor-intensive, this results in low efficiency, low accuracy, and poor real-time performance [1]. Thus, the traditional approach cannot satisfy the fabric quality and control requirements. As technology continues to mature, algorithms for fabric defect detection are emerging.

A number of fabric defect detection algorithms based on image segmentation have been proposed. Commonly used image segmentation methods include mathematical morphology [2], Fourier transforms [3], Gabor filters [4], gray level co-occurrence matrixes [5], and visual saliency [6]. Various studies [7]–[9] based on wavelet transforms and wavelet reconstruction algorithms can segment fabric defects effectively, although the selection of structural elements

is complicated. Gabor filtering [10], [11] is fairly robust but not accurate for textures that are similar to the background. An improved fabric defect detection method based on Fourier transform has been proposed [12], [13]. In this method, the local spatial information of the signal is ignored because it separates fabric defects and background textures with a global scope. Combining image segmentation with neural networks, a series of defect detection methods have been proposed. For instance, a new defect detection method for artificial neural networks has been trained using backpropagation algorithms [14]. The good time–frequency localization characteristics of wavelet transforms have been combined with the multi-scale image analysis function of fabric defect extraction and neural network technology to identify fabric defects accurately [15]. For another, a new method for defect detection using fabric multi-resolution decomposition has been proposed [16], though this has low accuracy and efficiency for defects with little background texture.

With the development of mechanism modeling, fabric defect detection algorithms based on saliency analysis have been developed. The center defined by Itti *et al.* [17] utilizes multi-scale image features, that is, the saliency of the image is obtained by considering the surrounding differences. Visual saliency analysis can quickly search for salient areas or

---

The associate editor coordinating the review of this manuscript and approving it for publication was Mehul S. Raval .

targets in images without prior knowledge using the human visual cognitive mechanism. A top-up approach has been used to construct the saliency map, with defects segmented according to some threshold [18]. However, the detection effect is not ideal for defect with low significance. Gofer-man *et al.* [19] and Huang *et al.* [20] applied context-based visual saliency analysis to target detection in natural scenes and achieved satisfactory results. A fabric image defect detection algorithm was developed [21] based on local statistical features and global significance analysis. A method has been reported that extracts global features from the input image from bottom to top, then extracts local features using the improved Itti saliency mapping model, and finally performs feature fusion [22]. Unfortunately, the effect of this method is not ideal when the defect saliency mapping is weak. A significant mapping of fabric defects has been developed in which a threshold is set and the fusion method segments the defects, but this is not ideal for the detailed detection of defects [23].

This paper analyzes the regional characteristics of fabric surface defects. Firstly, we pretreat the image and construct a significant mapping of fabric defects using a regional membership function, which separates the background texture from the defects. Second, an iterative threshold method and morphological processing are used to remove the influence of noise and background information, which improves the accuracy of fabric defect detection.

II. PRELIMINARIES
A. EXTREME POINT THEORY
In an image, the extreme points represent the high-luminance and low-luminance regions of the image. The maximum or minimum point of the image is assumed to be a defect or noise; otherwise, it is a background point [24]. That is,

$$f(x, y) = \begin{cases} 1, & f(x, y) \text{ is the extreme point} \\ 0, & f(x, y) \text{ is a non} - \text{extreme point} \end{cases} \quad (1)$$

B. ITERATIVE THRESHOLD METHOD
In the iterative selection method, an initial threshold is estimated firstly, and then the threshold through multiple calculations of the image is improved. By repeating the thresholding operations and segmenting the image into object and background classes, the threshold is finally improved using the gray classes in each class [25].

The basic steps of the iterative selection threshold method are as follows:

Step 1: Select an initial estimate of $T_0 = \{T_k \mid k = 0\}$. In this study, T_0 is the mean of the maximum gray value Z_{max} and the minimum gray value Z_{min}, namely,

$$T_0 = \frac{Z_{max} + Z_{min}}{2} \quad (2)$$

Step 2: The image is divided into two regions R_1 and R_2 using the threshold T_k:

$$\begin{cases} R_1 = \{f(x, y) \mid f(x, y) \geq T_k\} \\ R_2 = \{f(x, y) \mid 0 < f(x, y) < T_k\} \end{cases} \quad (3)$$

Step 3: The average gray values μ_1 and μ_2 are calculated for all pixels in each region R_1 and R_2:

$$\begin{cases} \mu_1 = \dfrac{\sum\limits_{f(i,j)<T_k} f(i, j) \times N(i, j)}{\sum\limits_{f(i,j)<T_k} N(i, j)} \\ \mu_2 = \dfrac{\sum\limits_{f(i,j)>T_k} f(i, j) \times N(i, j)}{\sum\limits_{f(i,j)>T_k} N(i, j)} \end{cases} \quad (4)$$

where $f(i, j)$ is the gray value of point (i, j) on the image and $N(i, j)$ is the weight coefficient of point (i, j). In this study, $N(i, j) = 0$.

Step 4: Calculate the new threshold T_{k+1}:

$$T_{k+1} = \frac{\mu_1 + \mu_2}{2} \quad (5)$$

Step 5: Repeat steps 2-4 until $T_{k+1} = T_k$ in successive iterations.

C. OPEN AND CLOSED OPERATIONS
The open and closed operations are compounded by the operations of expansion and corrosion in different orders. The open operation is eroded firstly and then expanded, and the closed operation is the opposite [26].

The definition of the open operation is as follows:

Using the structural element S, perform the open operation on A, denoted $A \circ S$. This can be expressed as:

$$A \circ S = (A \ominus S) \oplus S \quad (6)$$

The definition of the closed operation is as follows:

The closed operation of A using the structural element S, denoted as $A \cdot S$, can be expressed as:

$$A \circ S = (A \oplus S) \ominus S \quad (7)$$

D. SALIENCY OF IMAGE
Saliency refers to a pattern of image partitioning in machine vision, and a saliency map is an image that shows the uniqueness of each pixel. Image saliency is an important visual feature in any image, reflecting the importance to human eyes of certain image regions. Since the work of Guan and Gao [18], a large number of saliency mapping methods have been developed. In Fig. 1(a), the symbol "×" attracts people's attention quickly. It is more likely to attract attention because of the strong stimulation and the stimulation of new ideas.

III. PROPOSED METHOD
By analyzing the characteristics of the defect region and combining the idea of membership functions in fuzzy set theory, the saliency of the defect region can be improved, allowing the saliency mapping of the regional features to be constructed. The process of fabric defect detection and segmentation is shown in Fig. 2. Steps such as preprocessing, median difference and extremum retrieval, feature saliency
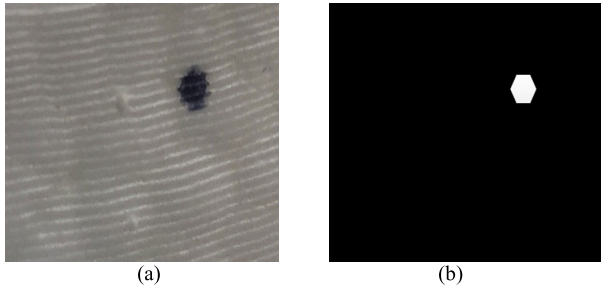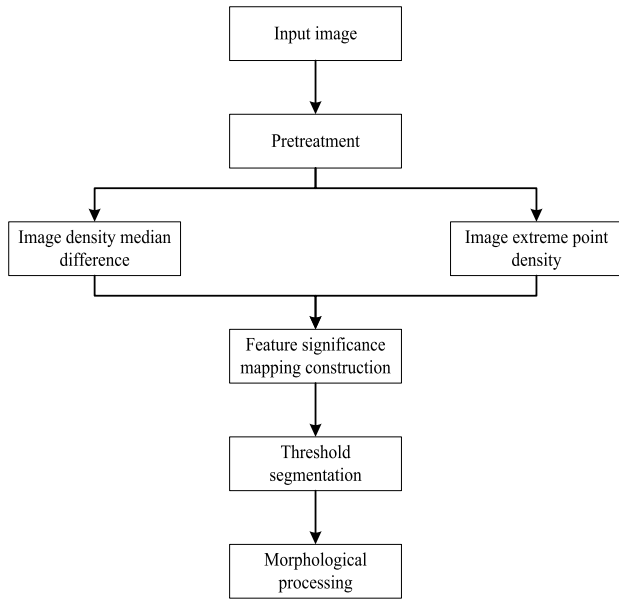
FIGURE 1. Example of image saliency.

FIGURE 2. Steps of fabric defect detection.

FIGURE 3. Gray histogram and gray density function graph. (a) Gray histogram; (b) gray density function graph.

mapping construction, threshold segmentation, and morphological processing are applied to the input image to enable the accurate detection of fabric defects.

A. PRETREATMENT

Images are easily polluted by all kinds of interference in their acquisition or transmission. To suppress the interference of noise information on the detection process, a 3×3 median filter is used to preprocess the original image and reduce the interference of noise.

B. SALIENCY MAPS CONSTRUCTION

A gray histogram of an image is an approximate representation of the density function of the gray image. At the boundary between the defect area and the texture background area, there is a significant change in the gray function. The mutation point is found using the extreme point function of the image, that is, the boundary point between the defect area and the background area. As the fabric defect area is much smaller than that of the background texture, the feature area is used to find the target area. By changing the weight of the
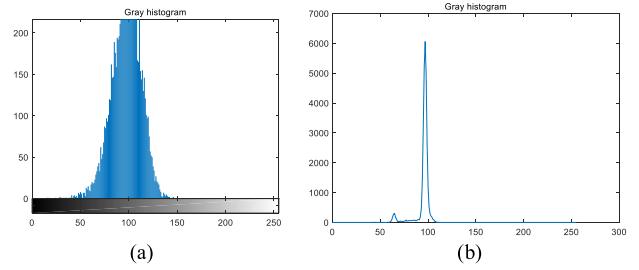
defect area and the background texture, the defect area can then be effectively segmented from the background texture.

1) GRAY DENSITY FUNCTION

For an image of size $M \times N$, the gray density function of the image is expressed as follows:

$$\begin{cases} if\ f\,(x, y) = i,\, i \epsilon\, [0, 255] \\ m\,(i) = num(f\,(x, y)) \end{cases} \quad (8)$$

$$p\,(i) = \frac{m\,(i)}{M \times N} \quad i \in [0, 255] \quad (9)$$

The gray histogram of the image and the gray density function of the image obtained by the above formula are shown in Figs. 3(a) and 3(b), respectively.

2) MEDIAN DIFFERENCE GRADIENT OF GRAY DENSITY FUNCTION

The median difference gradient of the gray density function can be expressed as:

$$\nabla p\,(t) = \frac{p\,(t + 2) - p(t)}{2} \quad t \in [0, 253] \quad (10)$$

The image is stored in digital form in a computer, that is, the image is a discrete digital signal. The gradient of the digital image is replaced by a differential in the continuous signal. A larger gradient indicates a greater change between the gray levels, converting the segmentation point between the fabric defect and the background texture to the extreme point of the curve of the gray density function. The median difference gradient of the gray density function is shown in Fig. 4.

3) GRAY DENSITY EXTREME VALUE

The extreme point is usually characterized by large changes, representing the boundary points or noise between the foreground and background, and can be used to determine the high- and low-brightness areas of the image. The segmentation points of fabric defects and background texture are converted to identify the mutation points in extremum density maps. Combined with extreme point theory, the gray density image extreme value can be defined as

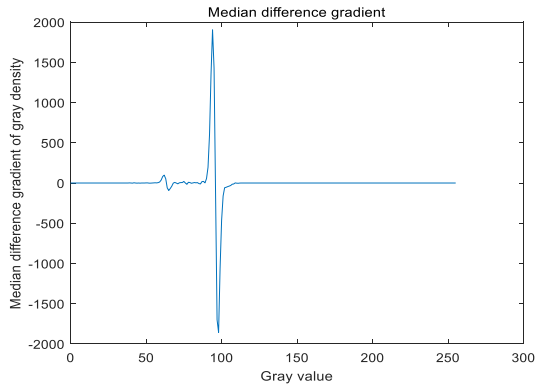$$f_E\,(x, y) = f_{Emax}\,(x, y) + f_{Emin}\,(x, y) \quad (11)$$

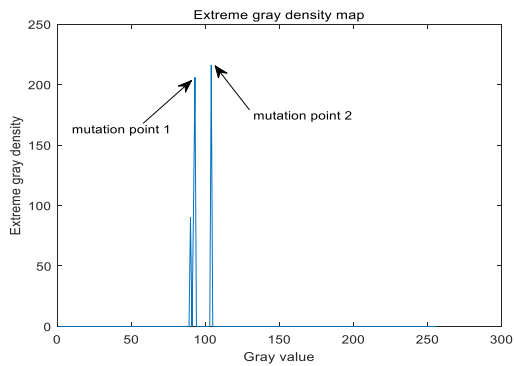**FIGURE 4.** Median difference gradient of the gray density function.

FIGURE 5. Extreme value of gray density map.

FIGURE 6. Differential gradient function graph after normalization.

where $f_E(x, y)$ represents all extreme points in the image, $f_{Emax}(x, y)$ represents all maxima in the image, and $f_{Emin}(x, y)$ represents all minima in the image. The extreme gray density map of the image is shown in Fig. 5.

4) CONSTRUCTION OF REGIONAL FEATURE MEMBERSHIP FUNCTION
Let the gray value of image $f(x, y)$ be t, and let t_1 and t_2 denote the maximum and second-highest peaks in the extreme values of the gray density map, respectively. In order to speed up the optimal solution of gradient descent, the characteristic function is constructed by combining membership function. A regional feature membership function is obtained by the following steps:

First, the median difference gradient obtained by (10) is subjected to extreme value normalization processing:

$$P(t) = |\frac{\nabla p(t) - min(\nabla p)}{max(\nabla p) - min(\nabla p)}| \quad (12)$$

The image of the differential gradient function after normalization is shown in Fig. 6.

Fuzzy theory [27] describes a degree of uncertainty that is measured by a membership function. Because of the uncertainty of the probability of occurrence of the background texture, the proposed method uses a sinusoidal membership function as the regional feature function. To study the segmentation effect of the background texture and defect region,
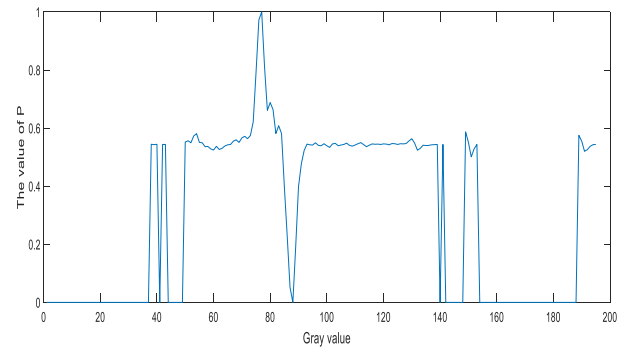
a segmentation coefficient α is introduced. To find the best segmentation effect, let $f(x, y) = t$, where $t \in [0, 255]$, and then

$$\begin{cases} r_1(x, y) = a * [1 - \sin(P(t))], & t \in [0, t_1] \\ r_2(x, y) = (1 - a) * sin(P(t)), & t \in (t_1, t_2) \\ r_3(x, y) = a * [1 - \sin(P(t))], & t \in [t_2, 255] \end{cases} \quad (13)$$

When $t \in [0, t_1]$, higher values of $r_1(x, y)$ indicate a greater possibility of $f(x, y)$ being the defect point; when $t \in [t_1, t_2]$, higher values of $r_2(x, y)$ indicate a greater possibility that $f(x, y)$ is part of the background texture; when $t \in [t_2, 255]$, higher values of $r_3(x, y)$ indicate a greater likelihood that $f(x, y)$ is a defect.

5) SIGNIFICANT IMPROVEMENT
Under the premise that the background texture and defect area are completely segmented, the defect area is guaranteed to have the strongest saliency. A weight coefficient β is introduced to improve the significance of regional features. The optimal effect of the defect area saliency can be obtained by adjusting the value of β during experiments.

$$\begin{cases} f(x, y) = 255 - (1 - \beta) \\ \quad \times f(x, y) \times r_1(x, y), & t \in [0, t_1] \\ f(x, y) = \beta \times f(x, y) \times r_2(x, y), & t \in [t_1, t_2] \\ f(x, y) = 255 - (1 - \beta) \\ \quad \times f(x, y) \times r_3(x, y), & t \in [t_2, 255] \end{cases} \quad (14)$$

According to (14), when $t \in [0, t_1]$, $f(x, y)$ may be part of the defect and its feature value is enhanced; when $t \in [t_1, t_2]$, $f(x, y)$ may be part of the background texture and its feature value is reduced; when $t \in [t_2, 255]$, $f(x, y)$ may be part of the defect and its feature value is enhanced.

C. THRESHOLD SEGMENTATION
The most common and simple Otsu method obtains the segmentation threshold using the maximum between-cluster variance. As the image surface defect area is smaller than the texture background area, the image segmented by this method cannot achieve satisfactory results. In this study, the iterative selection threshold method is used to segment the saliency
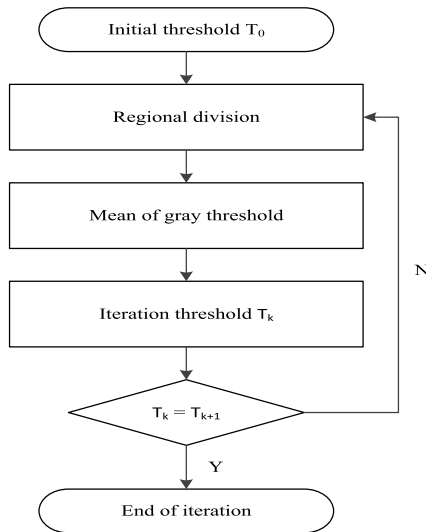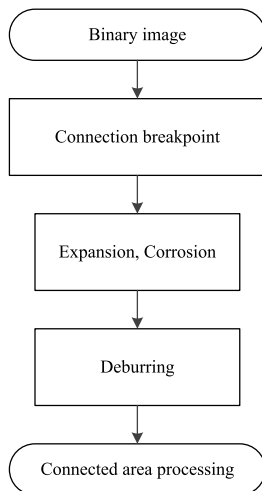
FIGURE 7. Threshold segmentation steps.

FIGURE 8. Main steps of morphological filtering.

map image. The main steps of threshold segmentation are shown in Fig. 7.

D. MORPHOLOGICAL FILTERING

As the defect area contains some noise and small outliers after segmentation, the binary image is subjected to corrosion and expansion to reduce the influence of this noise on the defect extraction. Connection and deburring are used to remove the outliers from the image, and some breakpoints are also connected so that the noise and outliers in the image can be effectively suppressed. The main steps of morphological filtering are shown in Fig. 8.

IV. EXPERIMENTAL RESULTS AND ANALYSIS
A. EXPERIMENTAL ENVIRONMENT
To verify the performance of the proposed method with various fabric defects, experiments were conducted using test images taken from the literature [23]; the size of each image

was 256×256 pixels. The experiments were performed on a PC with an Intel(R) Core(TM) i7-5500U CPU@2.40 GHz, 8 GB memory, and 64-bit Windows 10 OS. The experimental process used MATLAB R2016a.

B. SIGNIFICANCE ANALYSIS OF REGIONAL FEATURES
To study the completeness and saliency of the defect region and background texture segmentation, the segmentation coefficient α and weight coefficient β were introduced into the area feature weight function and the saliency improvement based on the region feature weight. Each experiment was repeated with various values of α and β. The degree of segmentation and significance are shown in Fig. 9.

When $\beta = 0$ and 0.5, an increase in α results in less complete segmentation; when $\beta = 1$ and 1.5, any increase in α gradually enhances the segmentation effect. When $\alpha = 0$, an increase in β reduces the saliency of the defect area; when $\alpha = 0.5$, the same occurs, and the saliency of the background texture also decreases. When $\alpha = 1$ and 1.5, an increase in β enhances the features of the defect area and reduces the saliency of the background texture. In summary, the best image segmentation effect is achieved when $\alpha = 1.5$ and $\beta = 1.5$.

C. ANALYSIS OF SURFACE DEFECT DETECTION RESULTS
Using the extreme point gray density function and linear function conversion, the values of the segmentation coefficient α and weight coefficient β were adjusted to construct a saliency map of the defect region. Threshold segmentation was applied to the saliency maps using iterative thresholding, and a binary image was finally obtained by morphological filtering. The experimental results given by the proposed algorithm (EPA) were compared with those from the traditional wavelet reconstruction algorithm (WRA) and the detection results of the TPA algorithm [23]. The detection results of the three algorithms are shown in Fig. 10.

As shown in Figs. 10(a), 10(b), and 10(d), WRA can only detect part of the defect information and the final image contains some noise. For smoother defect images, TPA only detects part of the information and small details of the defect. While removing the noise, EPA not only removes the background texture and defects, but also improves the detection accuracy.

D. ANTI-NOISE ANALYSIS
To verify the anti-noise performance of the proposed algorithm, Gaussian white noise of different intensities was added to the images (mean $\mu = 0$, different values of the variance σ). The anti-noise effects of the proposed algorithm were again compared with those of the WRA and TPA algorithms [23]. The results are shown in Fig. 11.

In Fig. 11, as the noise intensity increases from 2–20, the proposed algorithm achieves better detection results for most of the defect information, and effectively eliminates the noise. The WRA algorithm [23] loses its detection ability when
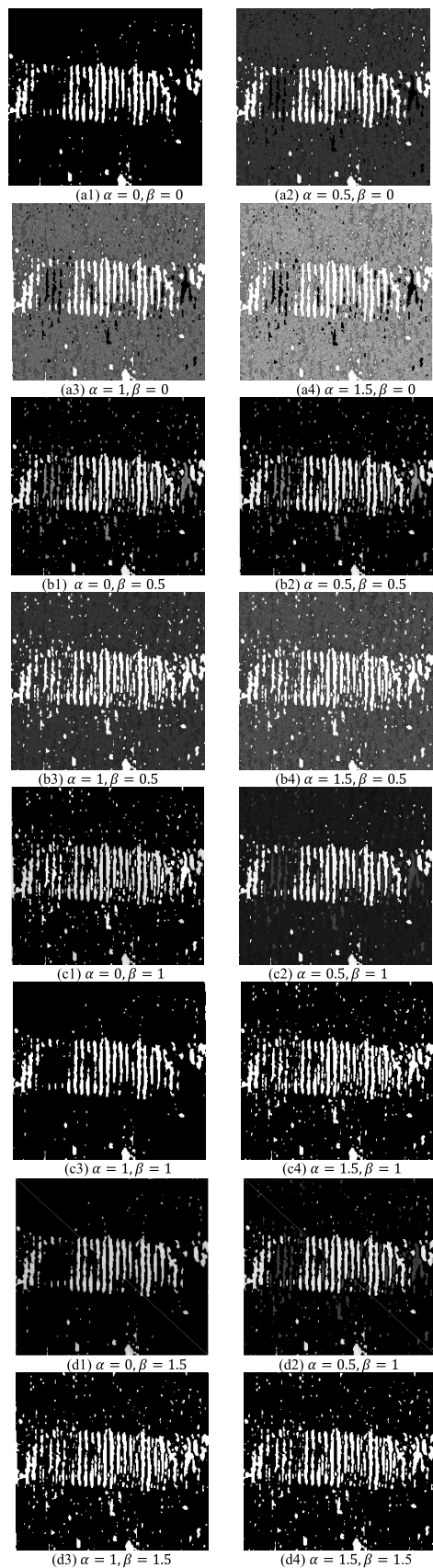
FIGURE 9. Characteristic saliency mapping of different partition coefficients and feature weight coefficients.

(a1) $\alpha = 0, \beta = 0$
(a2) $\alpha = 0.5, \beta = 0$
(a3) $\alpha = 1, \beta = 0$
(a4) $\alpha = 1.5, \beta = 0$
(b1) $\alpha = 0, \beta = 0.5$
(b2) $\alpha = 0.5, \beta = 0.5$
(b3) $\alpha = 1, \beta = 0.5$
(b4) $\alpha = 1.5, \beta = 0.5$
(c1) $\alpha = 0, \beta = 1$
(c2) $\alpha = 0.5, \beta = 1$
(c3) $\alpha = 1, \beta = 1$
(c4) $\alpha = 1.5, \beta = 1$
(d1) $\alpha = 0, \beta = 1.5$
(d2) $\alpha = 0.5, \beta = 1$
(d3) $\alpha = 1, \beta = 1.5$
(d4) $\alpha = 1.5, \beta = 1.5$
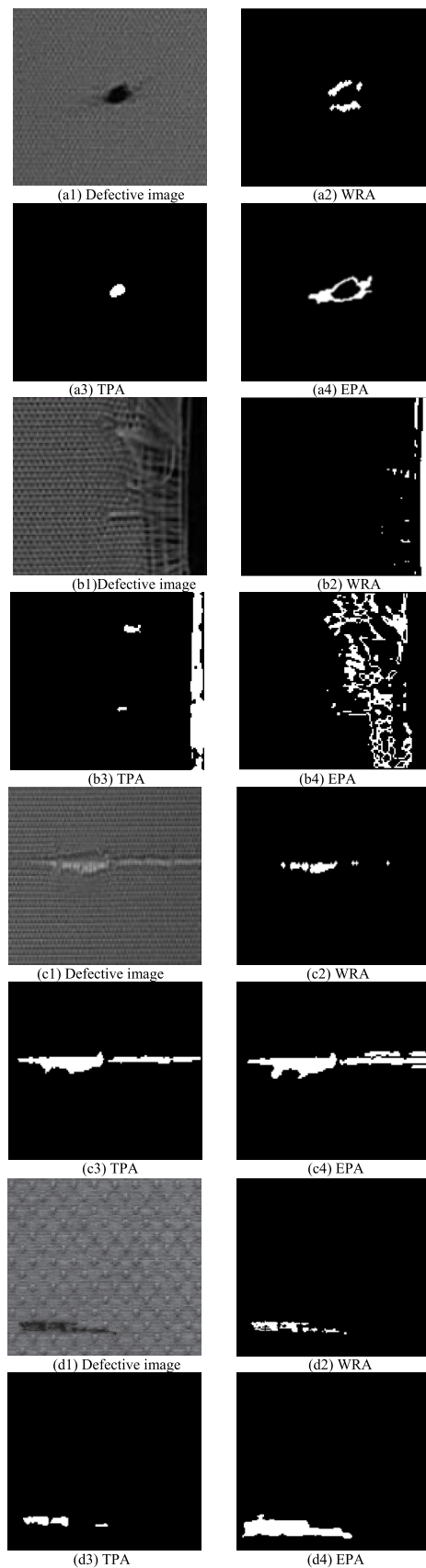
FIGURE 10. Effect of segmentation.

(a1) Defective image
(a2) WRA
(a3) TPA
(a4) EPA
(b1) Defective image
(b2) WRA
(b3) TPA
(b4) EPA
(c1) Defective image
(c2) WRA
(c3) TPA
(c4) EPA
(d1) Defective image
(d2) WRA
(d3) TPA
(d4) EPA

(a1)$\sigma = 2$, Noise image

(a2)$\sigma = 5$, Noise image

(a3)$\sigma = 10$, Noise image

(a4)$\sigma = 20$, Noise image

(b1)$\sigma = 2$, WRA

(b2)$\sigma = 5$, WRA

(b3)$\sigma = 10$, WRA

(b4)$\sigma = 20$, WRA

(c1)$\sigma = 2$, TPA

(c2)$\sigma = 5$, TPA

(c3)$\sigma = 10$, TPA

(c4)$\sigma = 20$, TPA

(d1)$\sigma = 2$, EPA

(d2)$\sigma = 5$, EPA

(d3)$\sigma = 10$, EPA

(d4)$\sigma = 20$, EPA
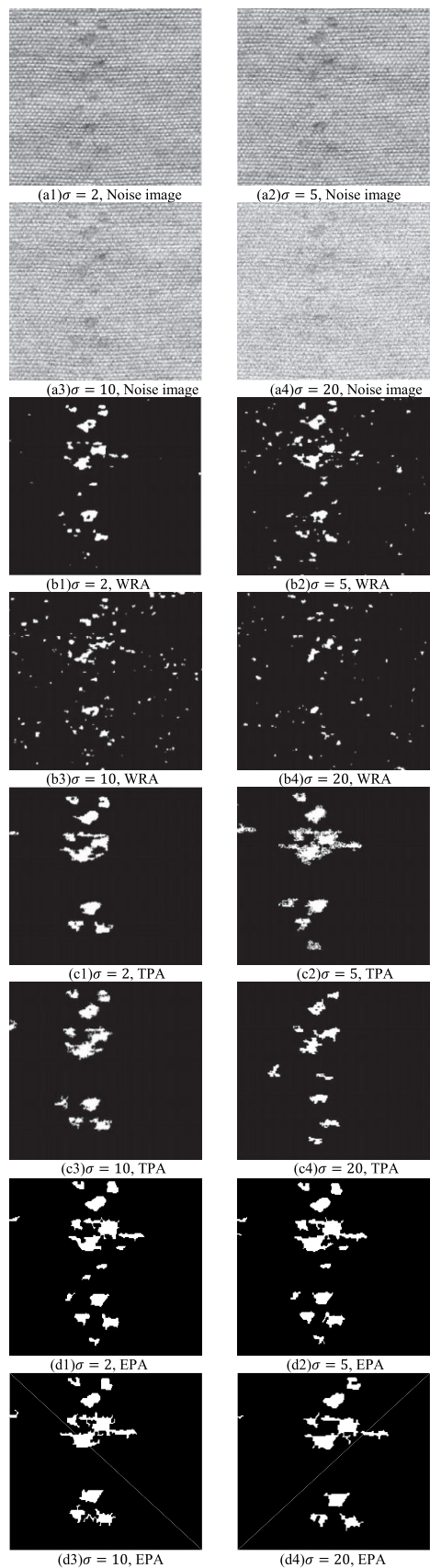
FIGURE 11. Segmentation results with different noise intensities.

(a) Miscellaneous defects

(b) Detection effect

(c) Dirty defect

(d) Detection effect

(e) Burnt defect

(f) Detection effect

(g) Flash defect

(h) Detection effect

(i) Dirty defect

(j) Detection effect

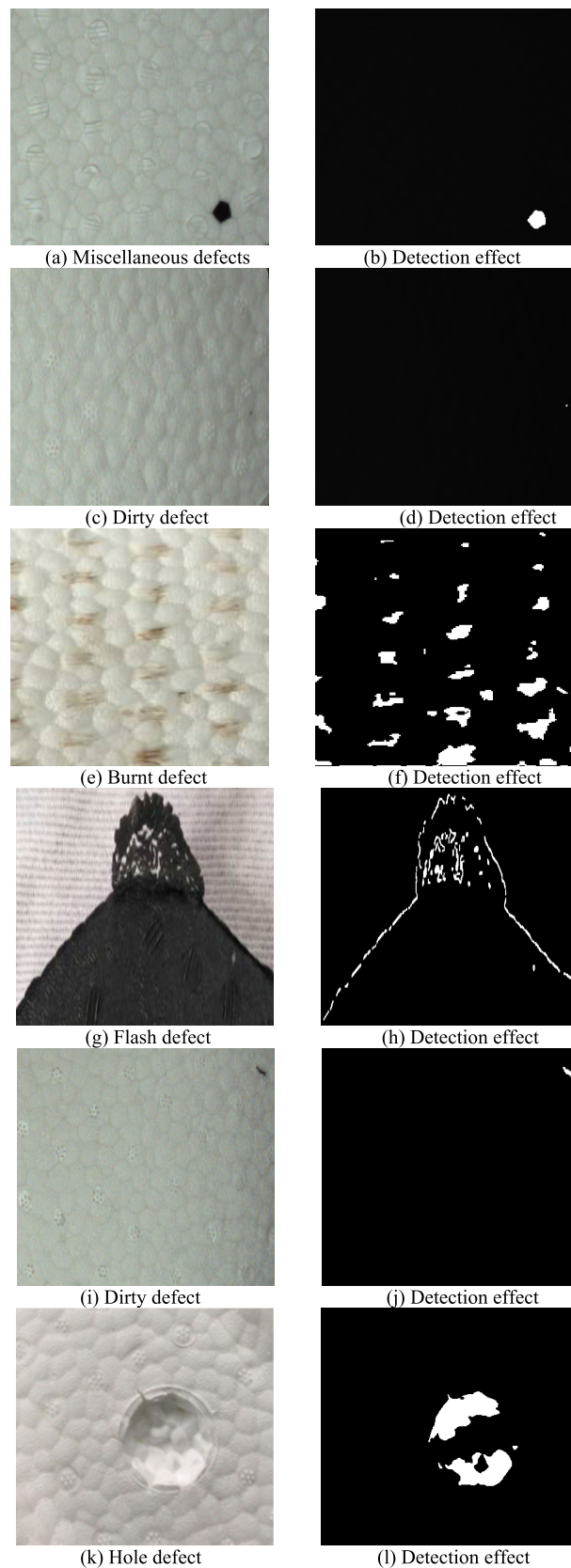(k) Hole defect

(l) Detection effect

FIGURE 12. ETPU shoe midsole material defect detection.

TABLE 1. Average runtime for different defect types.

image	WRA(s)	TPA(s)	EPA(s)
Point defect	1.62	1.51	0.97
Line defect	1.66	1.56	0.96
Linear defect	1.68	1.58	0.97
Scattered defects	1.68	1.58	1.08

TABLE 2. Accuracy of defect classification in this paper.

Image type	Number of samples	WRA (%)	TPA (%)	EPA (%)
Point defect	112	91.07	93.75	96.43
Line defect	164	88.41	93.90	95.12
Linear defect	156	83.33	96.15	97.44
Scattered defects	183	81.97	97.27	95.63
No defects	125	90.4	94.4	92.8

TABLE 3. Comparison with results in [23].

Image type	Number of samples	WRA (%)	TPA (%)	EPA (%)
Spreading defects	100	80	96	95
Local defect	100	92	99	99
Directional defect	100	89	97	98
No defects	100	90	97	96

the noise intensity is greater than 10, and the TPA algorithm detects less defect information.

E. RUNTIME ANALYSIS

To verify the effectiveness of the proposed algorithm, fabric defects were classified into point defects, line defects, and scattered defects according to their visual characteristics on the surface of the fabric. A defect detection experiment was performed using the proposed method, WRA, and TPA [23]. The runtimes of the various algorithms for each type of defect is summarized in Table 1.

F. DEFECT DETECTION ACCURACY ANALYSIS

To verify the accuracy of the detection of various fabric defects, the following accuracy index was defined:

$$acc = \frac{num(def)}{num(all)} \qquad (15)$$

where $num(def)$ represents the number of images for which a defect type can be accurately detected, $num(all)$ represents the number of images containing a particular defect type, and acc represents the accuracy obtained using this index.

Accuracy experiments were performed on the experimental images for different types of defects. The accuracy detection results are presented in Table 2; a comparison with the experimental results in [23] is given in Table 3.

G. APPLICABILITY ANALYSIS

To verify the applicability of the proposed algorithm, the detection performance with other materials was examined. As an example, the detection effect of ETPU shoe sole material defects is shown in Fig. 12.

V. CONCLUSION

By analyzing the saliency of the regional features of an image, this paper has presented a saliency mapping fabric defect detection method based on regional membership. This algorithm is not only applicable to fabric images with various degrees of roughness, but also introduces the extreme value method, a membership function, a segmentation coefficient and a weight coefficient. Thus, compared with WRA and TPA, the proposed approach offers enhanced background texture and defect segmentation and significant improvements in detection accuracy and robustness to noise. The proposed method can also separate various fabric defects with potential of high-standard detection of fabric defects.

REFERENCES

[1] B. Tang, J. Y. Kong, and S. Q. Wu, "Review of surface defect detection based on machine vision," *J. Image Graph.*, vol. 22, no. 12, pp. 1640–1663, 2017.

[2] K. L. Mak, P. Peng, and K. F. C. Yiu, "Fabric defect detection using morphological filters," *Image Vis. Comput.*, vol. 27, no. 10, pp. 1585–1592, Sep. 2009.

[3] K. Hanbay, M. F. Talu, and Ö. F. Özgüven, "Fabric defect detection systems and methods—A systematic literature review," *Optik*, vol. 127, no. 24, pp. 11960–11973, Dec. 2016.

[4] L. Tong, W. K. Wong, and C. K. Kwong, "Differential evolution-based optimal Gabor filter model for fabric inspection," *Neurocomputing*, vol. 173, pp. 1386–1401, Jan. 2016.

[5] B. Mingde, S. Zhigang, and L. Yesong, "Co-occurrence matrix and support vector description data," *Inf. Technol. J.*, vol. 11, no. 6, pp. 673–685, 2012.

[6] C. Gu and W. Ge, "Character recognition based on template matching method," *Commun. Technol.*, vol. 42, no. 6, pp. 220–222, 2009.

[7] H. Y. T. Ngan, G. K. H. Pang, S. P. Yung, and M. K. Ng, "Wavelet based methods on patterned fabric defect detection," *Pattern Recognit.*, vol. 38, no. 4, pp. 559–576, Apr. 2005.

[8] D.-M. Tsai and B. Hsiao, "Automatic surface inspection using wavelet reconstruction," *Pattern Recognit.*, vol. 34, no. 6, pp. 1285–1305, Jun. 2001.

[9] S. Guan, J. Yuan, and K. Ma, "Fabric defect detection based on wavelet reconstruction," in *Proc. Int. Conf. Multimedia Technol.*, Jul. 2011, pp. 3520–3523.

[10] Z. Chen and X. Feng, "The design of optimal real Gabor filters and their applications in fabric defect detection," *Coloration Technol.*, vol. 131, no. 4, pp. 279–287, Aug. 2015.

[11] Y. B. Liu, Z. T. Xiao, F. Zhang, and J. Wu, "Fabric defect detection method based on Gabor filters," *Adv. Mater. Res.*, vols. 301–303, pp. 229–234, Jul. 2011.

[12] C.-H. Chan and G. K. H. Pang, "Fabric defect detection by Fourier analysis," *IEEE Trans. Ind. Appl.*, vol. 36, no. 5, pp. 1267–1276, 2000.

[13] V. Jayashree and S. Subbaraman, "Identification of twill grey fabric defects using DC suppressed Fourier power spectrum sum features," *Textile Res. J.*, vol. 82, no. 14, pp. 1485–1497, Sep. 2012.

[14] P. Mitropoulos, C. Koulamas, R. D. Stojanovic, S. Koubias, G. D. Papadopoulos, and G. Karayanis, "Real-time vision system for defect detection and neural classification of Web textile fabric," *Proc. SPIE*, vol. 3652, pp. 59–69, Mar. 1999.

[15] Z. Kang, C. Yuan, and Q. Yang, "The fabric defect detection technology based on wavelet transform and neural network convergence," in *Proc. IEEE Int. Conf. Inf. Autom. (ICIA)*, Aug. 2013, pp. 597–601.

[16] Y. A. Karayiannis, R. Stojanovic, P. Mitropoulos, C. Koulamas, T. Stouraitis, S. Koubias, and G. Papadopoulos, "Defect detection and classification on Web textile fabric using multiresolution decomposition and neural networks," in *Proc. 6th IEEE Int. Conf. Electron., Circuits Syst. (ICECS)*, vol. 2, Sep. 1999, pp. 765–768.

[17] L. Itti, C. Koch, and E. Niebur, "A model of saliency-based visual attention for rapid scene analysis," *IEEE Trans. Pattern Anal. Mach. Intell.*, vol. 20, no. 11, pp. 1254–1259, 1998.

[18] S. Guan and Z. Gao, "Fabric defect image segmentation based on the visual attention mechanism of the wavelet domain," *Textile Res. J.*, vol. 84, no. 10, pp. 1018–1033, Jun. 2014.

[19] S. Goferman, L. Zelnik-Manor, and A. Tal, "Context-aware saliency detection," *IEEE Trans. Pattern Anal. Mach. Intell.*, vol. 34, no. 10, pp. 1915–1926, Oct. 2011.

[20] Z. Huang, F. He, X. Cai, Z. Zou, J. Liu, M. Liang, and X. Chen, "Efficient random saliency map detection," *Sci. China Inf. Sci.*, vol. 54, no. 6, pp. 1207–1217, Jun. 2011.

[21] Z. Liu, Q. Zhao, C. Li, Y. Dong, and L. Yan, "Fabric defect detection algorithm using local statistic features and global saliency analysis," *J. Textile Res.*, vol. 35, no. 11, pp. 62–67, 2014.

[22] G. Li, J. Shi, H. Luo, and M. Tang, "A computational model of vision attention for inspection of surface quality in production line," *Mach. Vis. Appl.*, vol. 24, no. 4, pp. 835–844, May 2013.

[23] S. Guan and H. Shi, "Fabric defect detection based on the saliency map construction of target-driven feature," *J. Textile Inst.*, vol. 109, no. 9, pp. 1133–1142, Sep. 2018.

[24] X. Zhang, Z. Zheng, I. Asanuma, and Y. Xu, "A new kind of hybrid filter based on the intersecting cortical model and the improved extremum-and-median filter," *Artif. Life Robot.*, vol. 19, no. 2, pp. 115–119, Sep. 2014.

[25] B. Zhao, L.-X. Zheng, X.-L. Pan, H.-T. Zhou, and Y.-Y. Xu, "New approach of fabric defects detection based on saliency region feature," *J. Comput. Appl.*, vol. 32, no. 6, pp. 1574–1577, Apr. 2012.

[26] J. G. M. Schavemaker, M. J. T. Reinders, J. J. Gerbrands, and E. Backer, "Image sharpening by morphological filtering," *Pattern Recognit.*, vol. 33, no. 6, pp. 997–1012, Jun. 2000.

[27] L.-K. Huang and M.-J.-J. Wang, "Image thresholding by minimizing the measures of fuzziness," *Pattern Recognit.*, vol. 28, no. 1, pp. 41–51, Jan. 1995.

LIWEN SONG received the B.E. degree in information and computing science from Hubei Minzu University, China, where he is currently pursuing the M.S. degree in operational research and cybernetics with the School of Mathematics and Statistics. His research interests mainly focus on digital image processing and JAVA programming.

RUIZHI LI received the B.E. degree in civil engineering from the Beijing University of Civil Engineering and Architecture, in 2018. He is currently pursuing the M.S. degree in operational research and cybernetics with the School of Mathematics and Statistics, Hubei Minzu University, China. His research interests are mainly in digital image processing and MATLAB programming.

SHIQIANG CHEN received the B.S. degree in mathematics from Hubei Minzu University, in 1997, the M.S. degree in computer software and theory from Guizhou University, in 2005, and the Ph.D. degree in computer science and technology from Sichuan University, in 2017. He is currently a Professor with the School of Advanced Materials and Mechatronic Engineering, Hubei Minzu University. His research interests mainly focus on software technology, network communication, image engineering, and the Internet of Things.

• • •